Electric control of a {Fe_4} single-molecule magnet in a single-electron transistor

J. F. Nossa,[1,2] M. F. Islam,[1] C. M. Canali,[1] and M. R. Pederson[3]

[1]*Department of Physics and Electrical Engineering, Linnaeus University, SE-39182 Kalmar, Sweden*

[2]*Solid State Physics/The Nanometer Structure Consortium, Lund University, Box 118, SE-221 00 Lund, Sweden*

[3]*Office of Basic Energy Sciences, SC22.1,U. S. Department of Energy, 1000 Independence Ave. SW, Washington, DC 20585-1290, USA*

(Received 13 March 2013; revised manuscript received 9 October 2013; published 26 December 2013)

Using first-principles methods, we study theoretically the properties of an individual {Fe_4} single-molecule magnet (SMM) attached to metallic leads in a single-electron transistor geometry. We show that the conductive leads do not affect the spin ordering and magnetic anisotropy of the neutral SMM. On the other hand, the leads have a strong effect on the anisotropy of the charged states of the molecule, which are probed in Coulomb blockade transport. Furthermore, we demonstrate that an external electric potential, modeling a gate electrode, can be used to manipulate the magnetic properties of the system. For a charged molecule, by localizing the extra charge with the gate voltage closer to the magnetic core, the anisotropy magnitude and spin ordering converges to the values found for the isolated {Fe_4} SMM. We compare these findings with the results of recent quantum transport experiments in three-terminal devices.

DOI: 10.1103/PhysRevB.88.224423 PACS number(s): 75.50.Xx, 75.30.Gw, 75.75.−c, 73.23.−b

I. INTRODUCTION

In recent years, molecular spintronics has emerged as one of the most active areas of research within magnetism at the atomic scale.[1–6] Progress in the field is driven in part by advances in chemical design and synthesis, which allow the realization of interesting magnetic molecules with desired electronic and magnetic properties. A second essential feature of ongoing research is the improved ability of integrating individual magnetic molecules into solid-state nanoelectronic devices.

Typically, magnetic molecules have long spin-relaxation times, which can be utilized in high-density information storage. They are also usually characterized by a weak hyperfine interaction with the environment, resulting in long spin-coherence times, which is an essential property for applications in quantum information processing. Single-molecule magnets (SMMs) are a special class of spin-ordered and/or magnetically active molecules characterized by a relatively high molecular spin and large magnetic anisotropy energy.[7] The latter lifts the spin degeneracy even at zero magnetic field, and favors one particular alignment of the spin, making the molecule a nanoscale magnet.

One of the goals of molecular spintronics is to address the magnetic states of individual magnetic molecules with electric fields and electric currents. In the last six years, experimental efforts toward this goal have considered different classes of magnetic molecules and strategies to incorporate them into electric nanocircuits. A particularly interesting direction focuses on quantum transport in a single-electron transistor (SET), a three-terminal device where a SMM bridges the nanogap between two conducting nanoleads, and can further be electrically manipulated by the gate voltage of a third nearby electrode. In the regime of weak coupling to the leads, the electric charge on the central SMM is quantized and can be controlled by the external gate. When Coulomb blockade is lifted by either gate or bias voltages, transport occurs via tunneling of single electrons in and out of the SMM. Therefore, a study of transport in this geometry can provide detailed information on the magnetic properties of individual SMMs, both when the molecule is neutral and when it is electrically charged.

Early SET experiments on SMMs (Refs. 8 and 9) focused on the archetypal SMM {Mn_{12}} acetate,[7,10] characterized by the ground-state spin $S = 10$ and a large magnetic anisotropy barrier of approximately 50 K. Unfortunately, these experiments and studies of self-assembled molecules on gold surfaces[11] have shown that the magnetic properties of {Mn_{12}} complexes are extremely fragile and easily disrupted when the molecule is attached to metallic leads or surfaces.

More recently, another class of SMMs, namely the tetranuclear {Fe_4} molecule, has emerged as a candidate in molecular spintronics that does not suffer the drawbacks of {Mn_{12}}. The properties of {Fe_4} in its neutral state are well studied in the crystal phase[12,13] and include a molecular ground-state spin $S = 5$ and an intermediate magnetic anisotropy barrier $\approx$15 K. In contrast to what happens with {Mn_{12}}, these magnetic characteristics remain stable when the molecule is deposited on a gold surface.[14,15] Furthermore, its tripodal ligands are shown to be advantageous for the preparation of single-molecule electronic devices. Indeed, recent three-terminal quantum transport experiments,[16–18] with {Fe_4} as the central island of a SET, show that this molecule behaves indeed as a nanoscale magnet, even when it is wired to metallic leads. The magnetic anisotropy is significantly affected by adding or subtracting single charges to the molecule,[16] an operation that can be performed reversibly with the gate voltage. More refined techniques[18] allow the extraction of the magnetic anisotropy of the neutral and charged molecule from the transport measurements with unprecedented accuracy.

In this paper, we carry out density functional theory (DFT) calculations to evaluate the magnetic properties of a {Fe_4} connected to gold electrodes and under the effect of an external electric field representing a gate voltage. The geometry considered here is supposed to model the typical situation realized in current SET experiments, although some details might be different. The main aim of our work is to investigate theoretically how the spin ordering and the

magnetic anisotropy of $\{Fe_4\}$ are affected by weak coupling to the leads, both when the molecule is in its neutral state and when a single charge is added to or subtracted from the device. A second important objective of the paper is a theoretical analysis of how these magnetic properties can be modified and controlled by means of an external electric potential representing a gate electrode.

Although a full-fledged first-principles study of quantum transport is beyond the scope of this paper, as we explain in the following, we believe that our analysis of the charged states under the effect of an external electric field is useful to develop methods to compute the tunneling conductance within a master-equation formalism. Reference 19 introduced a DFT description of the neutral and charged states of an *isolated* $\{Mn_{12}\}$ SMM, which were then used in a master-equation formalism for quantum transport. Here, the coupling to the leads was treated phenomenological tunneling amplitudes taken from experiment. In Ref. 20, charge transport through a Mn_{12} SMM attached to two Au electrodes was studied in the regime of strong coupling between molecule and leads, by means of a nonequilibrium Green's function (NEGF) approach combined with density functional theory. Similar approach and techniques were used in Ref. 21 to investigate the bias-dependent transport properties of the same system in the strong coupling regime. It was shown[21] that hybridization of the Mn_{12} SMM energy levels in an external electric field generates features in the I-V curves that depend on the internal spin configuration of the molecule. Transport calculations carried out in the same transport regime using NEGFs but based on microscopic tight-binding models have also been considered.[22] The approach based on NEGFs, suitable for strong coupling, has the drawback that charging effects, essential for the description of SET experiments, can not be adequately incorporated.

In this sense, this paper is a further contribution to these early attempts to use first-principles methods based on DFT to investigate quantum transport in a SET with a SMM. We are aware that the use of DFT can be problematic when it comes to describing the electronic structure and Fermi level alignment of molecules coupled to external electrodes, particularly when charged states are involved. Assessing the limitations of DFT in this context is also a technical aim of this paper. In this regard, we discuss potential uncertainties in the relative level alignment of the electrode and molecular states.

The main findings of our analysis are the following. The SMM $\{Fe_4\}$ in its neutral state is indeed quite robust against the presence of metallic leads: both spin ordering and magnetic anisotropy are essentially identical to the one of the isolated molecule. For the case of a charged molecule, the effect of the leads is more complex. Our calculations show that the extra charge tends to reside primarily on the ligands between molecule and metallic leads, and only minimally on the magnetic core. As a result, the addition of electrons affects the magnetism of the molecule (specifically the magnetic anisotropy) considerably less than when the molecule is isolated. We find that an external gate voltage can be used to localize the extra charge closer to the central magnetic core, and in this case the magnetic characteristics of the device converge to those of the isolated $\{Fe_4\}$ SMM. Some details of the results presented here might depend on the ligands used to attach the molecule to the leads. The choice adopted here is quite typical and in part suggested by experimental work on magnetic molecules functionalized on Au surfaces and SET devices. Nevertheless, other variations, involving different chemical entities, are possible, and their effect on the properties of the system should be further investigated.

The organization of this paper is as follows. In Sec. II, we present an overview of the theoretical and computational approach employed in this work. The electronic and magnetic properties of different charge states of the isolated $\{Fe_4\}$ SMM is discussed in Sec. III. The effects of the metallic leads on the properties of the molecule are discussed in Sec. IV. In Sec. V, we discuss how a confining electric potential affects the magnetic properties of the molecule. In Sec. VI, we compare the results of our calculations with recent SET transport experiments. Finally, in Sec. VII we summarize our results.

II. THEORETICAL BACKGROUND

A. Spin Hamiltonian and the giant-spin model

In a first approximation, the exchange interaction between the magnetic ions of a molecular magnet can be described by an isotropic Heisenberg model

$$H = \sum_{ij} J_{ij} \mathbf{s}_i \cdot \mathbf{s}_j, \tag{1}$$

where $\mathbf{s}_i$ is the spin of the magnetic ion i and the constants J_{ij} describe the superexchange coupling between ions i and j. Clearly, the validity of Eq. (1) relies crucially on the assumption that each magnetic ion is characterized by a well-defined quantum spin, localized at the ion position. There might be cases where the spin polarization of the molecule is delocalized, where this assumption may break down. Such cases are especially probable when an excess tunneling electron is present. Once the exchange constants are known, the Hamiltonian can be diagonalized. Since H is a sum of scalars in spin space, it commutes with the total spin $\mathbf{S}$. Therefore, the eigenvalues of $\mathbf{S}^2$ and S_z can be used to label the eigenstates of H.

In the case of single-molecule magnets, the ground state (GS) of Eq. (1) is characterized by a relatively large spin S, and it is separated by a fairly large energy $\Delta J \equiv \mathrm{Max}_{\{ij\}}[J_{ij}]$ from excited states with different total spins. Thus, at low energies $< \Delta J$ the magnetic molecule behaves effectively as an atom with a relatively large spin S, known as *giant spin*. The approximation of restricting to the lowest-spin multiplet is known as *giant-spin model*. According to Eq. (1), each spin multiplet is degenerate. In the next section, we will discuss how spin-orbit interaction lifts this degeneracy, splitting the $2S + 1$ states of the GS multiplet.

Note that the ground-state spin S is not always the maximum value $S_{\max}$ allowed by Eq. (1). Due to the presence of antiferromagnetic components, the most common situation encountered in SMMs is an intermediate value $0 < S < S_{\max}$, which quasiclassically corresponds to a ferromagnetic spin configuration. Following, we will show how all the physical quantities entering in the spin Hamiltonian of Eq. (1) and the value of the giant spin S can be calculated within DFT.

B. Spin-orbit interaction and magnetic anisotropy barrier

Spin-orbit interaction introduces terms to Eq. (1) that break rotational invariance in spin space. Up to second-order perturbation theory, these terms, aside from anisotropic corrections to the Heisenberg model, include the antisymmetric Dzyaloshinskii-Moriya spin exchange and the single-ion magnetic anisotropy $H_{ia} = -\sum_i (\mathbf{d}_i \cdot \mathbf{s}_i)^2$. Because of these terms, the total spin is no longer a good quantum number. Within the giant-spin model of SMMs, where the isotropic exchange is the dominant magnetic interaction, the main effect of the spin-orbit interaction is to lift the spin degeneracy of the GS multiplet. To second-order perturbation theory, this can be described by the following anisotropy Hamiltonian for the giant-spin operator $\mathbf{S} = (S_x, S_y, S_z)$:

$$\mathcal{H} = DS_z^2 + E\left(S_x^2 - S_y^2\right). \tag{2}$$

The parameters D and E specify the axial and transverse magnetic anisotropy, respectively. If $D < 0$ and $|D| \gg |E|$, which are defining properties for SMMs, the system exhibits an easy axis in the z direction. In the absence of magnetic field, and neglecting the small transverse anisotropy term, the GS of Eq. (2) is doubly degenerate and it corresponds to the eigenstates of S_z with eigenvalues $\pm S$. To go from the state $S_z = +S$ to the state $S_z = -S$, the system has to climb an anisotropy energy barrier $\Delta E = |D|S^2$ via transitions to adjacent excited states with $|S_z| < S$. This corresponds to the energy barrier of the classical energy functional $\mathcal{H} = D\mathbf{S}^2\cos(\theta)^2$. When the transverse term is nonzero, S_z is not a good quantum number. The classical barrier separating the two degenerate minima is no longer $|D|S^2$ but smaller, and it decreases with increasing E. Indeed, classically, if E is not zero, one can rotate the moment through either the hard axis or the medium axis and obtain barriers that differ by DS^2. If $D > 0$, the systems have a quasieasy plane perpendicular to the z axis without energy barrier. Although the correct classical barrier is $(D - E)S^2$, in this paper we follow the experimental convention of referring to the classical barrier as DS^2 since E is usually very small.

The anisotropy parameters D and E can be calculated within a self-consistent-field (SCF) one-particle theory (e.g., DFT or Hartree-Fock), by including perturbatively the contribution of the spin-orbit interaction. In the Appendix, we summarize the main steps of the procedure originally introduced in Ref. 23. (For more recent reviews, see Refs. 24 and 25.)

The perturbative method described in the Appendix works well for systems with a large HOMO-LUMO gap. Here, HOMO and LUMO refer to the highest occupied molecular orbital and lowest unoccupied molecular orbital, respectively. However, for systems that have nearly degenerate and not fully occupied HOMO levels, which often is the case for charged molecules, the perturbative approach breaks down since some of the energy denominators in Eq. (A7) vanish. To avoid this problem, the magnetic anisotropy can alternatively be calculated by an exact diagonalization method. In this approach, the solutions of the one-particle Schrödinger equation in the SCF approximation (which does not include SOI), are used to construct a finite matrix representation of the SOI, which is then diagonalized exactly. The matrix is then diagonalized subject to the constraint that the resulting spin is aligned along a given choice of the quantization axis. The resulting single-particle solutions $\{\epsilon'_k, |\psi'_k\rangle = \sum_\sigma |\phi'_{k\sigma}\rangle|\chi_\sigma\rangle\}$ are used to compute the trace of the system as a function of direction of the quantization axis (or average direction of the magnetization). In Ref. 26, a discussion of the relationship between the second-order variation in the trace and the self-consistent second-order variation of total energy is presented.

Once one has obtained the trace as a function of axis of quantization, one can use relatively standard techniques to decompose the trace into a spherical harmonic representation and then determine the magnetic principal axes. Alternatively, by choosing magnetic principal axes that are equivalent to those predicted from the second-order expressions, it is always possible to directly compare exact-diagonalization results with the second-order results. Using exact diagonalization, one can further extract parts of the fourth- and higher-order anisotropy terms as well. However, since self-consistency and other terms also affect the magnetic anisotropy at fourth order and beyond, the exact diagonalization results are primarily used to determine whether the second-order results are expected to be stable and a good approximation to experiment. In cases where near degeneracies occur at the Fermi level, the second-order and exact-diagonalization results can be very different, especially if the states near the Fermi level are coupled by the spin-orbit interaction. For such cases, a much more careful analysis of results is needed and it is reasonable to expect that some degree of self-consistency with noncollinear capabilities will be needed.

For electronic-structure methods, such as the Naval Research Laboratory Molecular Orbital Library[27,28] (NRLMOL) used in this work, where the wave functions are expanded in terms of atom-centered localized basis functions, the second-order perturbative method allows one to further analyze the anisotropy Hamiltonian on an atom-by-atom basis. By expanding the Kohn-Sham orbitals ($|\phi_{k\sigma}\rangle$) in Eq. (A7) in terms of the atom-centered basis, the second-order expression [Eq. (A5)] can be decomposed into a sum over four centers.[29] The superdiagonal terms (all center indices the same) can then be used to determine an anisotropy Hamiltonian associated with each atom. In Ref. 29, this decomposition has been used to verify the perpendicular hard-axis alignment model in the Co_4 easy-plane magnetic molecule. In Ref. 30, Baruah's method was used to demonstrate that essentially all of the magnetism in Mn_{12} acetate was due to the outer eight $S = 2$ crown Mn ions, and that the sum of the single-ion anisotropies was very close to the total anisotropy. Further, the degree to which nonadditivity occurred was explained by a canting of the atom projected anisotropy axes relative to the global anisotropy axis.

To complete the discussion about second-order anisotropy Hamiltonians, derived either perturbatively or via exact diagonalization, it is important to note a contribution to van Wullen and co-workers.[31,32] Van Wullen noted that once a method is used to determine the spin-orbit energy as a function of axis of quantization that an additional quantum correction is needed to determine the parameter's D and E in the anisotropy Hamiltonian. For example, the $M_s = 0$ eigenstate is not aligned with an axis of quantization along the x axis, the y axis, or any other axis. Therefore, more care must be taken to determine D once the classical energy as a function of expectation value of $\mathbf{S}$ is known. Accounting for this correction

changes the definition of D, as originally derived by Pederson and Khanna, by a factor of $(S + 1/2)/S$. While this correction is small in the large-S limit, it can be important for systems with lower spin.

C. Computational details

In this paper, we use a self-consistent field approximation based on density functional theory (DFT). A review of this approach in the study of molecular magnets can be found in Ref. 25. Here, we recall a few key features that are relevant for this work.

In a DFT calculation of a magnetic molecule, we obtain the total energy of the system for specially prepared spin symmetry-breaking metastable states. In many cases these are ferromagnetic spin configurations, suggested by experiment. The energies of these different metastable states can then be compared and the lowest-energy spin configuration determined. Alternatively, it is also possible to impose a fixed spin configuration, which in principle would not remain stable after convergence. In all these symmetry-breaking calculations, the state with a given spin configuration is represented by a single Slater determinant of occupied single-particle states, constructed in terms of self-consistent Kohn-Sham eigenvectors. In the absence of SOI, the Kohn-Sham wave functions have a well-defined spin character, majority or minority spin. Therefore, the single Slater determinant, representing a given spin configuration, is an eigenstate of the component of the total spin $\mathbf{S}$ in the direction of the quantization axis $\hat{\mathbf{n}}$, which is the magnetization direction. In general, this single Slater determinant is not an eigenstate of $\mathbf{S}^2$, but in many cases it will have a large overlap with the eigenstate of $\mathbf{S}^2$ with S equal to the eigenvalue of $\mathbf{S} \cdot \hat{\mathbf{n}}$. The GS total spin S of the molecule (in the absence of SOI) is taken to be equal to one half of the excess of majority spin electrons $S = \Delta N/2 = (N_{\mathrm{maj}} - N_{\mathrm{min}})/2$ for the metastable spin configuration with the lowest total energy. The spin magnetic moment of the system in units of the Bohr magneton μ_{B} is then $\mu_S = \Delta N \mu_{\mathrm{B}} = 2S\mu_{\mathrm{B}}$. In the DFT study of SMMs the possible presence of fractional occupancy of some of the KS wave functions close to the Fermi energy might result in noninteger values of $N_{\mathrm{maj}} - N_{\mathrm{min}}$. Typically, this happens when the HOMO-LUMO gap is very small or vanishing. We will encounter examples of this difficulty in the study of the charged states of $\{Fe_4\}$. The existence of this general problem was first discussed by Janak *et al.*[33] in reference to near degeneracies between $3d$ and $4s$ electrons in neutral isolated atoms. More recent manifestations of this issue have been identified by Perdew *et al.* for systems where charge transfer is important.[34] In that work, Perdew *et al.* warn the reader that higher-level methods which include approximate self-interaction corrections are susceptible to dissociation into fractionally occupied systems. At present, this problem constitutes a significant practical and formal challenge to researchers that are interested in modeling transport processes in closed systems containing more than two atomic or molecular scale fragments with variable electronegativities. This is the situation occurring in the systems considered in this paper.

In Ref. 35, a set of equations was derived which, while cumbersome to solve, allow one to variationally determine the electronic occupations that satisfy the conditions proposed by Janak in Ref. 33. Unfortunately, that method is tedious and hard to implement in general. Others have proposed solutions that include nonzero temperature and entropy affects[36,37] from both numerical and formal points of view.

The DFT calculations discussed herein are performed with the Gaussian-orbital-based NRLMOL program.[27,28] All calculations employ the Perdew-Burke-Ernzerhof[38] (PBE) generalized-gradient approximation for the density functional. A large basis set is employed in which the exponents for the single Gaussians have been fully optimized for DFT calculations. The NRLMOL code employs a variational mesh for numerically precise integration and an analytic solution of Poisson's equation.

All-electron calculations are performed for all elements of the $\{Fe_4\}$ SMM except for the Au atoms that are used to construct the leads attached to the molecule, for which we have used pseudopotentials. All the electronic and magnetic properties are calculated using an optimized geometry. More specifically, most of the geometries in this work were optimized using the limited-memory Broyden-Fletcher-Goldfarb-Shanno method (LBFGS). However, for some of the cases where charge transfer from the leads to the island was sensitive to geometry, we switched to the conjugate-gradient method.

In connection with the issue of fractional occupancy mentioned above, we note that for the calculations presented here we have used a broadening temperature to minimize the energy as a function of occupation numbers for states that are nearly degenerate at the Fermi level. This type of problem can be particularly difficult for systems where charge transfer between the leads and the islands is sensitive to geometry. In all cases, the temperature (0.0001–0.003 a.u.) used for Fermi broadening was chosen to minimize the energy of the system. Therefore, we view our results as being as an idealization of zero temperature.

DFT can be used to extract the parameters defining the spin Hamiltonian that is supposed to describe the exchange interaction between the magnetic ions of the molecule. First of all, DFT can be used to ascertain whether or not there is a localized spin at each magnetic ion, by calculating the total spin polarization inside a sphere centered about a given atom. For typical SMMs, including the one considered in this paper, while the magnetization density is not localized entirely on the magnetic ions, the assumption of a well-defined quantum spin often turns out to be quite reasonable. Once this is established, the calculation of the total energy for a few spin configurations permits the computation of the exchange constants of Eq. (1). We will see an example of this in the next section.

III. ELECTRONIC AND MAGNETIC PROPERTIES OF ISOLATED $\{Fe_4\}$ SMM

The chemical composition of the molecule used in this work is $Fe_4C_{76}H_{132}O_{18}$.[12] The four Fe atoms in $\{Fe_4\}$ SMM form an equilateral triangle, as shown in Fig. 1. The molecule has idealized D_3 symmetry with the C_2 axis passing through the central atom and one of the peripheral atoms. Using first-principles methods, we have calculated, in detail, the electronic and the magnetic properties of the $\{Fe_4\}$ SMM.

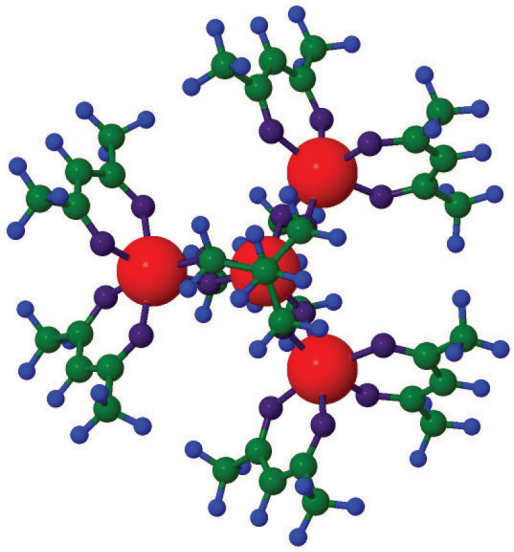

FIG. 1. (Color online) Ball-stick top view of an isolated {Fe$_4$} SMM. Red, green, blue, and purple balls correspond to iron, carbon, hydrogen, and oxygen atoms, respectively.

In the ground state, the central Fe atom is coupled antiferromagnetically with three peripheral atoms, whereas the three peripheral atoms are coupled ferromagnetically with each other, as shown in Fig. 2. Each of the four Fe atoms has spin $S_{\mathrm{Fe}} = \frac{5}{2}$, thus the total spin of the ground state is $S = 5$. The magnetic interactions between these atoms can be described by the Heisenberg spin Hamiltonian [Eq. (2)]

$$H = J(\mathbf{s}_1 \cdot \mathbf{s}_2 + \mathbf{s}_1 \cdot \mathbf{s}_3 + \mathbf{s}_1 \cdot \mathbf{s}_4) + J'(\mathbf{s}_2 \cdot \mathbf{s}_3 + \mathbf{s}_3 \cdot \mathbf{s}_4 + \mathbf{s}_4 \cdot \mathbf{s}_2). \quad (3)$$

The two exchange parameters J and J' can be written in terms of the expectation values of the Hamiltonian of Eq. (3), for different spin configurations

$$J = -\tfrac{2}{75}(E_{duuu} - E_{uuuu}),$$
$$J' = \tfrac{1}{75}(2E_{duuu} - 3E_{uudd} + E_{uuuu}). \quad (4)$$

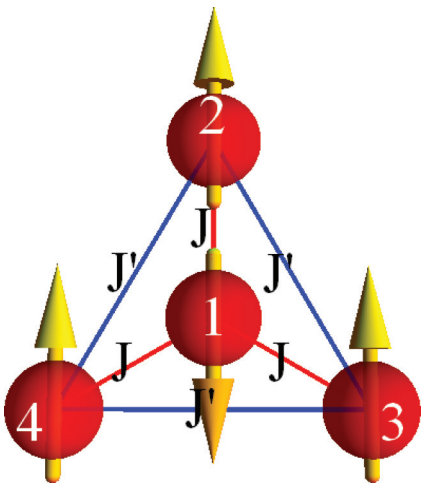

FIG. 2. (Color online) Exchange-interaction constants between four Fe atoms in {Fe$_4$} SMM.

TABLE I. Properties of the isolated {Fe$_4$} SMM for the three different charge states.

Charge state	Spin magnetic moment $\mu_S(\mu_B)$	HOMO-LUMO energy gap (eV)	Anisotropy barrier (K)
$Q = 0$	10.0	0.85	16.05
$Q = +1$	9.3	0.80[a]	53.42
$Q = -1$	9.0	0.06	1.88

[a]Note that the energy gap reported for the cation refers to the energy difference between the half-filled HOMO and empty LUMO. See Fig. 3(c).

Here, E_{duuu}, E_{dduu}, and E_{uuuu} are the energies of the molecule where the spin orientations at their respective atomic positions (1,2,3,4) are labeled as d = down or u = up. Using NRLMOL, we have calculated the energies of different spin configuration and upon substitution in Eq. (4), we obtain $J = 9.94$ meV and $J' = 0.64$ meV. DFT calculations overestimate J and J' since estimated values from susceptibility measurements[39] are 2.62 and 0.14 meV, respectively. However, we note that the ratio of these two parameters agrees quite well for both theory and experiment. These values of the exchange constants ensure that the GS of the spin Hamiltonian (4) has indeed a total spin $S = \frac{5}{2}$, well separated from excited states characterized by other values of S.

Using first-principles methods, we have calculated the electronic and magnetic properties of {Fe$_4$} SMM for the neutral ($Q = 0$) and two charged states, namely, the anion ($Q = -1$) and the cation ($Q = +1$). (We will refer to the value Q as the *extra charge* added to the system.) A summary of the results is shown in Table I. These results can be understood with the help of the structure of the single-particle energy levels around the Fermi level in the absence of SOI, plotted in Fig. 3 for the three charge states $Q = 0, \pm 1$.

The neutral molecule has a stable $S = \frac{5}{2}$ GS, as anticipated. The HOMO-LUMO gap of the neutral isolated Fe$_4$ molecule is about 0.85 eV, where both HOMO and LUMO levels are

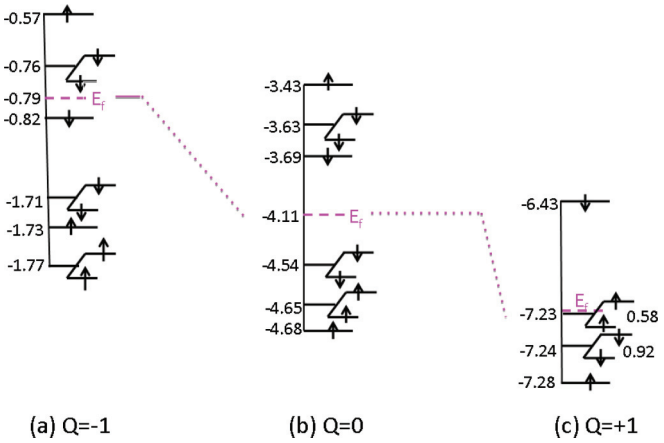

FIG. 3. (Color online) Energy levels (eV) of different charge states of isolated the {Fe$_4$} SMM without spin-orbit coupling. E_f represents the Fermi level. The numbers on the right of the HOMO and HOMO-1 levels in (c) are the fractional occupancies of the corresponding level.

minority- (down-) spin states [see Fig. 3(b)]. Apart from a small swapping of two levels below the HOMO, the level structure for the $Q = -1$ charge state can be obtained from the energy levels of the neutral system simply by filling the neutral LUMO with a spin-down electron [see Fig. 3(a)]. As a result, the total spin of the anion is $S = \frac{9}{2}$. Note also that the HOMO-LUMO gap of the anion is now reduced to 0.06 eV compared to the neutral molecule. The electronic states change significantly for the $Q = +1$ charge (cation) state: the two doubly degenerate spin-up HOMO-1 and spin-down HOMO states of the neutral molecule swap place [see Fig. 3(c)]. Furthermore, since there is now one fewer electron, the new HOMO is now half-filled. This implies that the total spin of the cation is again reduced with respect to the neutral molecule by $\frac{1}{2}$, that is, $S = \frac{9}{2}$. The fractional occupancy of the HOMO plays an important role in the enhancement of the magnetic anisotropy, discussed in the following. Our DFT calculations yield values of the total spin S in agreement with the level structure of Fig. 3. In particular for the charged states $Q = \pm 1$, even when the initial spin configuration is set to be $S = \frac{11}{2}$, the system converges eventually to the value $S = \frac{9}{2}$.

For the neutral molecule, the magnetic anisotropy landscape is characterized by an easy axis in the direction perpendicular to the plane containing the four Fe atoms (the z axis). As shown in Table I, we find that the anisotropy barrier for this case is about 16 K, which is in agreement with previous calculations.[40] (In Ref. 40, the authors have used two different $\{Fe_4\}$ complexes. The molecular symmetry for one of these complexes is C_2, whereas the the other one has D_3 symmetry. Our calculations agree well with the one that has D_3 symmetry.) Note that a well-defined energy gap between occupied and unoccupied states (regardless of the spin) ensures that the perturbative and exact calculation of the anisotropy coincide.

The magnetic anisotropy of the $Q = +1$ charge state has also uniaxial character in the z direction, with a barrier of about 53 K, significantly larger than that obtained for the neutral molecule. On the other hand, for the $Q = -1$ charge state the anisotropy is reduced to about 1.9 K, with an easy axis in the XY plane of the Fe atoms.[41] The large change in the anisotropy for the two charged states has a very different origin for the two cases and can be understood in the following way.

For the $Q = -1$ case, the small gap between the like-spin HOMO and LUMO states might at first suggest a breakdown of the perturbative treatment. In fact, these two states are coupled only minimally by SOI. The most important coupling occurs between the spin-down HOMO and the spin-up LUMO+1 states. The energy difference between these two states is $\approx$0.25 eV. This value and the corresponding energy denominator in Eq. (A7) are large enough for perturbation theory to work (as a comparison with the exact approach clearly shows) and, at the same time, small enough for this individual transition to completely determine the main features of the anisotropy landscape. In particular, it turns out that this term in Eq. (A7) favors an easy axis along a direction in the XY plane of the Fe atoms. Since this magnetization direction is unfavorable for other terms in Eq. (A7) (which prefer the z direction), there are positive and negative contributions in the total-energy difference for the two magnetization directions [calculated with Eq. (A5)], which in the end lead to a reduced anisotropy barrier.

The large enhancement of the magnetic anisotropy barrier found for the $Q = +1$ state can also be understood with the help of the single-particle energy diagram shown in Fig. 3(c). We observe that the half-filled doubly degenerate spin-up HOMO level lies just above a (close-to-100%) filled doubly degenerate spin-down HOMO-1 level. The term involving transitions between these two occupied and unoccupied levels totally dominates Eq. (A7). In fact, the smallness of the corresponding energy denominator (a few meV) renders the perturbative approach inadequate. This is a classical example of a quasidegeneracy at the Fermi level, where the exact treatment of SOI is necessary. As it is often the case, the inclusion of SOI lifts the quasidegeneracy for a particular direction of the magnetization, leading to a substantial decrease of the total energy for that direction and, consequently, to a large anisotropy energy barrier.

IV. $\{Fe_4\}$ SMM ATTACHED TO METALLIC LEADS

In this section, we investigate how the electronic and magnetic properties of the $\{Fe_4\}$ SMM change when the molecule is attached to metallic leads, as in transport experiments. The system that we have in mind is a single-electron transistor device, where metallic nanoleads, separated by a nanogap created by either break junction or electric migration, are bridged by a molecule functionalized with convenient chemical ligands.

First, in our theoretical modeling we are forced to find a convenient finite representation of otherwise semi-infinite leads in the form of finite clusters. For the calculations reported in this paper we have chosen to model a metallic nanolead with a finite cluster of 20 gold (^{79}Au) atoms, arranged in a special tetrahedral structure, which can be viewed as a fragment of the face-centered-cubic lattice of bulk Au (see Fig. 4). This metal cluster, Au_{20}, has been previously investigated by Li *et al.* in Ref. 42, where it was shown that 20 Au atoms arranged in this geometric configuration form a very stable system. Its very

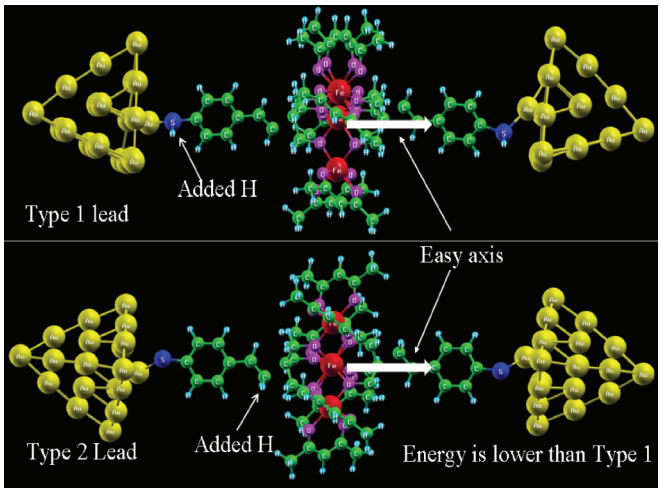

FIG. 4. (Color online) $\{Fe_4\}$ SMM connected to Au_{20} leads. Two types of leads are used in these calculations. In the type-1 lead, a H atom is added to the S atom near the gold lead (top figure). In the type-2 lead, a H atom is added to a C atom in the phenyl group near the $\{Fe_4\}$ molecule (bottom figure).

large HOMO-LUMO gap (1.77 eV) makes Au_{20} chemically very inert. What is also important is that its unique tetrahedral structure makes this cluster an ideal model for Au surfaces at the nanoscale.

In fact, the tetrahedral Au_{20} is the best representation of bulk Au at the nanoscale. It is known, for example, that this cluster, at least qualitatively, already shows all the characteristics of the bulk band of gold.[43] Our DFT calculations find that the ionization potential of Au_{20} is 7.3 eV to be compared with work function of gold, which is 5.1 eV. The bulk work function can be viewed as the ionization of an infinite cluster. This should differ from that of a finite cluster by approximately $27.2116/R$ (2.86 eV) where $R = 9.5$ bohrs is approximately the radius of the cluster. Our rationale for using this cluster to model metal leads is that during the fabrication of the nanometer-spaced electrodes, via self-breaking by electromigration for example, the ensuing Au nanoleads will relax into the most stable configuration which might be well described by tetrahedral Au_{20}.

Second, since ultimately we would like to investigate transport properties of this system in the Coulomb blockade regime, it is essential that coupling between the leads and molecule is weak. After constructing the two leads in the form of two Au_{20} clusters, we have connected the molecule via phenyl groups, as shown in Fig. 4. The functionalization of the ligands of {Fe_4} SMM by means of phenyl groups is well known and suitable to attach the molecule to Au surfaces.[12,15]

A similar (but not identical) way of connecting the {Fe_4} SMM to Au leads is employed in SET experiments in the Coulomb blockade regime,[16–18] and it ensures that the electronic coupling between the molecule and electrodes is weak. To maintain proper bonding and ionic neutrality of the entire cluster, we have further removed one hydrogen (H) atom from the molecule close to the contact point and have added it to the ligand part of the cluster. We have considered two different ways of doing this. In the first case (hereafter called type-1 lead), we have added the H atom to the sulfur (S) atom near the Au cluster. In the second case (hereafter called type-2 lead), we have added H to the carbon (C) atom near the contact point as shown in Fig. 4. After connecting the leads with the molecule, we have relaxed the entire system again. Typically, we find that the system with type-2 leads is more stable, that is, its energy is approximately 0.6 eV lower than the energy of the system with type-1 leads. We will nevertheless report results for both cases unless otherwise specified. The two types of linkers adopted here should be viewed as a theoretical modeling of standard experimental realizations presently in use. Other variations obtained by modifying the details of the chemical composition of the ligands are possible, but will not further be pursued here. The effect of these modifications on the magnetic properties is the subject of future research.

A summary of the magnetic properties of the neutral molecule attached to A_{20} leads is shown in Table II. We can see that the combined molecule plus leads system maintains a sizable HOMO-LUMO gap of about 0.75 eV. The first important result is that coupling the leads does not cause a change of the spin of the molecule, which remains equal to the value of the isolated neutral {Fe_4}, $S = 5$. Second, the leads have a very small effect also on the magnetic anisotropy of the system: the magnetic anisotropy landscape has still an easy axis along the same z direction (see white arrow in Fig. 4), with an energy barrier quite close to the 16 K of the isolated molecule.

TABLE II. Properties of neutral {Fe_4} SMM attached to A_{20} leads, compared to the properties of the isolated molecule (first row). Type 1 and type 2 (called in the paper also type-1 and type-2 leads) refer to the two different choices to place a hydrogen atom to the ligand (see Fig. 4).

	Spin magnetic moment $\mu_S(\mu_B)$	HOMO -LUMO gap (eV)	Anisotropy energy (K)
{Fe_4}	10	0.85	16.05
{Fe_4}+type 1	10	0.87	15.99
{Fe_4}+type 2	10	0.57	15.47

We can gain some insight about the robustness of the magnetic structure of {Fe_4} SMM under the influence of metallic contacts by investigating the changes in the single-particle energy levels and level alignment and occurring when the leads are connected to the molecule. We have calculated separately the energy levels of the isolated Au lead(s) and the {Fe_4} + phenyl group, along with the levels of the combined system [Au leads + {Fe_4} + phenyl group]. The results are shown in Fig. 5. The states at and near the Fermi level of the two subsystems are dominated by the d levels of Au atoms and the p levels of the C atoms of the phenyl group. Thus, when the two systems are combined, the charge transfer taking place to align the Fermi energies of the two subsystems is restricted only within the contact region, leaving the magnetic properties of the {Fe_4} inner core unchanged. Figure 5(b) shows that the

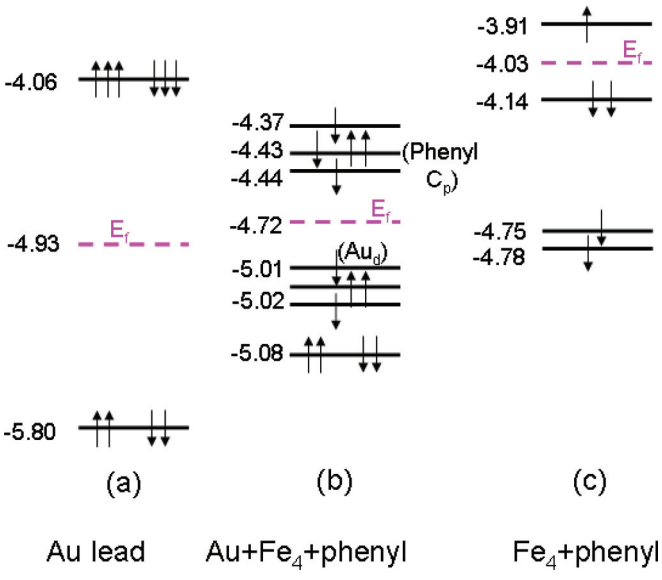

FIG. 5. (Color online) Shifts in the energy levels (eV) of neutral {Fe_4} SMM when connected to two Au_{20} leads (of type 2). Please note that the energies are not scaled. (a) Isolated Au lead, (b) leads + {Fe_4} + phenyl, and (c) {Fe_4} + phenyl. The labels Au_d and phenyl C_p in (b) indicate that the main contribution to those levels comes from d levels of the Au leads and p levels of C in the phenyl ligands, respectively.

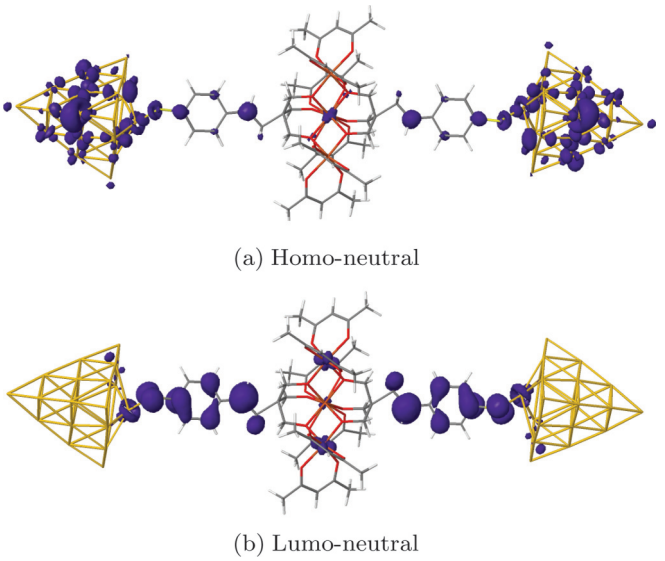

(a) Homo-neutral

(b) Lumo-neutral

FIG. 6. (Color online) HOMO and LUMO of the neutral molecule.

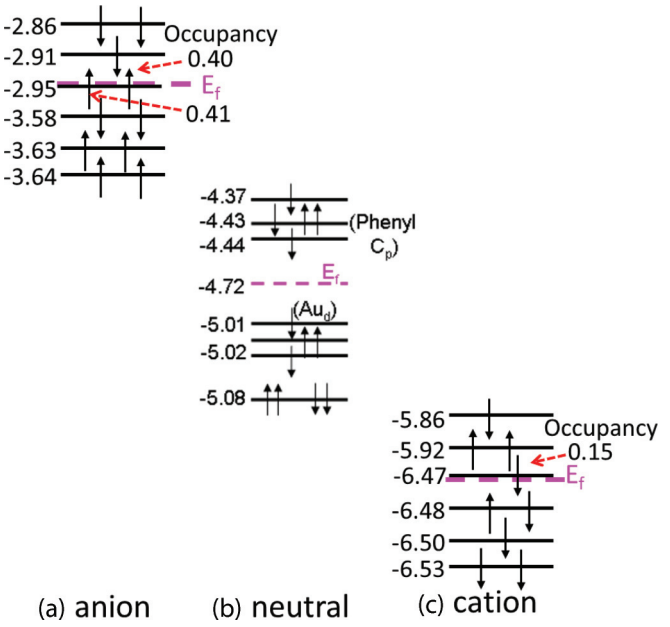

FIG. 7. (Color online) Energy levels (eV) for the three charge states $Q = 0, \pm 1$ for the $\{Fe_4\}$ SMM connected to two Au_{20} leads (of type 2). Please note that the energies are not scaled. (a) Anion. (b) Neutral [same as in Fig. 5(b)]. (c) Cation. The labels Au_d and phenyl C_p in (b) indicate that the main contribution to those levels comes from d levels of the Au leads and p levels of C in the phenyl ligands, respectively.

energy levels of the combined system close to the Fermi level correspond primarily to states remote from the magnetic core. This is also supported by Fig. 6, where we plot the probability density for the HOMO and LUMO states of the $\{Fe_4\}$ + leads system. Both states have negligible contributions on Fe atoms or atoms immediately nearby to these. As we will see in the following, this implies that the magnetic properties will remain unchanged even when extra charge is added to (or subtracted from) the system.

Figure 5(b) shows that both the nondegenerate spin-down HOMO and the nondegenerate spin-down LUMO of the neutral system lie quite close in energy to degenerate levels (occupied and nonoccupied, respectively). Therefore, we can expect that subtle energy-level swaps may occur when one electron is added to or subtracted from the system. As it is evident from Fig. 7, this is exactly what the calculations show. For the case of leads of type 2, the HOMO of the anion ($Q = -1$) is now a half-occupied doubly degenerate spin-up level, lying very close to a nondegenerate spin-down LUMO. This leads to a GS spin $S = \frac{11}{2}$, and to a spin magnetic moment close to $\mu_s = 11\mu_B$ (see Table III).[44] A similar situation occurs for the $Q = +1$ charge state, which has a GS spin $S = \frac{11}{2}$. We find that this state is, however, almost degenerate with another state with $S = \frac{9}{2}$. For leads of type 1 (which are less stable), the spin configurations $S = \frac{11}{2}$ and $\frac{9}{2}$ are almost degenerate for both charged states $Q = \pm 1$. Note that the spin magnetic moment of the $Q = -1$ charge state is now closer to $\mu_S = 9\mu_B$. The quasidegeneracy of two different spin configurations is a situation where the assumption of the existence of a well-defined giant-spin model may not be entirely adequate.

TABLE III. Magnetic properties of the three charge states when the $\{Fe_4\}$ SMM is attached to Au leads as in Fig. 4.

Charge state	Spin magnetic moment $\mu_S(\mu_B)$		Anisotropy energy (K)	
	Type 1	Type 2	Type 1	Type 2
$Q = 0$	10.0	10.0	15.99	15.47
$Q = +1$	9.0	10.95	17.73	14.74
$Q = -1$	9.6	10.65	11.23	16.97

As shown in the Table III, in contrast to the case of the isolated $\{Fe_4\}$ SMM where the anisotropy of the charged states are significantly different from that of the neutral molecule, when the leads are attached to the molecule the anisotropy energy of the charged states remains close to the value of the neutral system. We also note that magnetic properties of the charge states have some dependence on the type of the lead attached to the molecule.

As anticipated above, an explanation of this behavior is already suggested by the energy diagram of Fig. 5(b) and the plots of Fig. 6 demonstrating that both the HOMO and the LUMO of the neutral system are states predominately localized around the Au leads and within the phenyl group, respectively. Therefore, we expect that when we add or remove an electron from the system it largely resides in the lead and phenyl group, leaving the magnetic states in $\{Fe_4\}$ molecule relatively unchanged. The easy axis, in all cases, points perpendicularly to the Fe_4 plane, as shown in Fig. 4, except for $Q = -1$ charge state of type-1 lead, which is in the plane.

Further support to this picture is provided by calculating the real-space location of the extra charge when an electron is added or subtracted to the system. As an example, we consider here the case of the anion, where one electron is added to the system. Since part of this extra charge might end up in interstitial regions between atoms (this is the case for the extra charge on the Au leads), particular care must be taken in

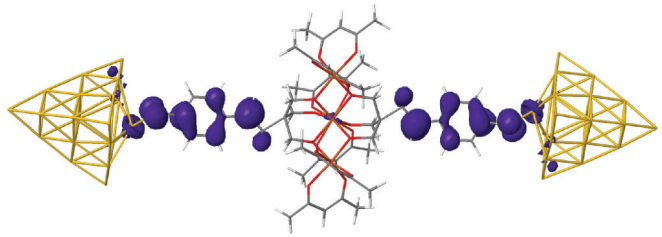

(a) HOMO 1

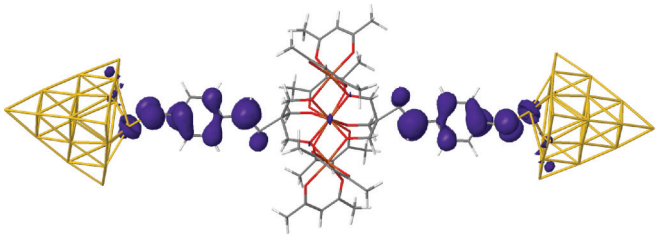

(b) HOMO 2

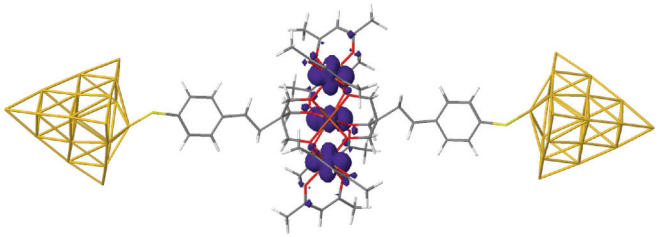

(c) LUMO

FIG. 8. (Color online) The two quasidegenerate HOMOs and the LUMO of the anion charge state. Approximately 20% of the HOMO wave functions reside on the Au leads, primarily on the interstitial space between Au atoms (see Fig. 9). This contribution is not visible on the scale of this plot.

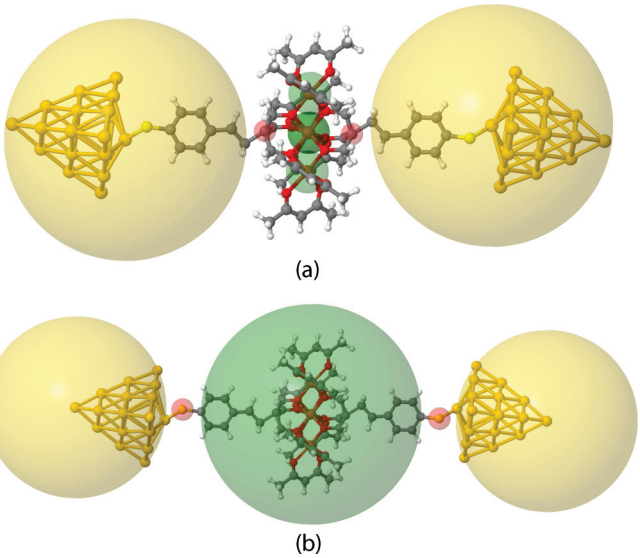

FIG. 9. (Color online) Evaluation of the fraction of extra charge for the anion state ($Q = -1$, one extra electron added) with respect to the neutral state, contained in different regions of the $\{Fe_4\}$ molecule plus leads and phenyl groups. In (a), each yellow sphere surrounding the lead and the phenyl group contains about 40% of an electron charge. In (b), each yellow sphere, surrounding only the Au lead, contains 21% of electron charge. Therefore, the amount of charge transferred to the leads is about 42% and to the phenyl groups is 38%. The rest of the extra charge ≈20% is in the $\{Fe_4\}$ region.

drawing conclusions based only on the atomic-position plot of the HOMO states, shown in Fig. 8, which might miss this contribution. To capture the interstitial contribution, we draw instead a large sphere enclosing a given region of the system. NRLMOL is able to calculate the extra charge contained globally in that region, including interstitial contribution. By repeating the same calculation with different spheres centered at different locations, we can eventually determine the amount of extra charge in different relevant parts of the system.

In Fig. 9(a), we consider a sphere (yellow color) containing both the lead and the phenyl group linker. We find that the amount of extra charge contained in this region is 40% of one electronic charge. The remaining 20% is located on atoms in the nearest surrounding of the $\{Fe_4\}$ core. In Fig. 9(b), the sphere encloses only the Au lead but no linker. For this case we find that each Au leads contains 21% of extra electronic charge. We conclude that when one electron is added to the system, a total of 42% of the extra charge resides on the leads, 38% on the ligands and only 20% is around the magnetic core of $\{Fe_4\}$. This 20% of added charge is not directly on the Fe atoms and therefore does not change the magnetic properties of $\{Fe_4\}$ significantly.

Further evidence of this important conclusion is provided by the comparison of the calculated local spin magnetic moments of the Fe atoms for the isolated $\{Fe_4\}$ molecule and for molecule-plus-lead system, for different charge states. The results are shown in Fig. 10. We note from the figure that for the isolated molecule the magnetic moments change considerably for the charged states, whereas for molecule plus lead system, the corresponding change is very small. Clearly, when the molecule is attached to the Au leads, adding or removing one unit charge affects the magnetic states of the $\{Fe_4\}$ minimally, which is also why we do not see a large change in magnetic anisotropy for different charge states.

We conclude this section with a few comments on the important issues of the nature of the charged states, and the coupling between molecule and leads, emerging from the DFT calculations. First, we have seen that when one electron is added or subtracted to the system $\{Fe_4\}$ + (finite) leads, the extra charge is predominantly localized on the ligands (≈40%) and on the leads (≈40%). If we could increase the size of the leads, a larger fraction of the extra charge would be likely to spread on the metallic leads. Therefore, one could argue that the charged states $Q = \pm 1$ investigated above are not a fully adequate description of the charged states involved in the sequential tunneling processes taking place in a SET, where the additional charge should be essentially localized on the central island. Second, and partly connected to this issue, the nonzero amplitude of the LUMO wave function of the neutral system (which is quite close to the HOMO wave function of the anion) seems to indicate that the ligands considered here do not behave as tunnel barriers of a SET, but rather model an example of strong coupling between molecule and leads.[45] Both these features could be

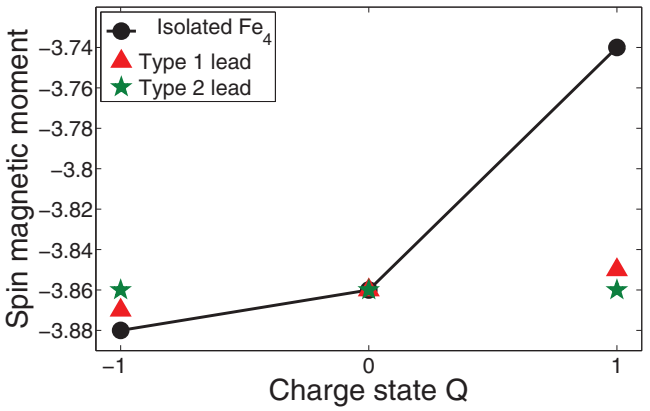

(a) Central Fe atom

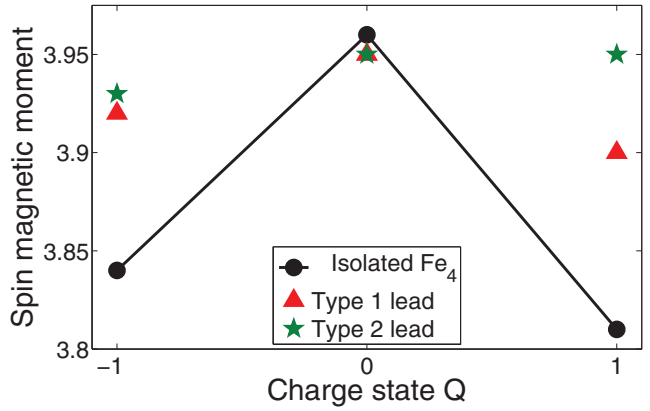

(b) Vertex Fe atoms

FIG. 10. (Color online) Local magnetic moments of Fe atoms. The negative and the positive moments in the two figures imply that moments of central and vertex atoms are opposite to each other.

due to limitations of the DFT approach considered here, which tends to overdelocalize any added charge. Such drawbacks can possibly be improved by more refined DFT treatments, involving, for example, self-interaction corrections. While we believe that these refinements are important and should be further investigated, the goal and strategy of this paper is to simulate with DFT a realistic example of SMM attached to leads, being aware of these limitations.

V. EFFECT OF AN EXTERNAL ELECTRIC POTENTIAL

In SET devices, the charge of the central island weakly coupled to metallic electrodes can be varied experimentally one by one by applying an external electric field via a third gate electrode, which overcomes the charging energy e^2/C of the island. Here, we investigate the effect of an external gate electrode, whose electric potential tends to confine the extra charge closer to the molecule. Note that in phenomenological studies of SETs based on model Hamiltonians, a gate voltage only shifts the energies of the isolated "quantum dot" without affecting its wave functions. As we show in the following, in our case the gate voltage can be used to localize a wave function closer to the molecule and modify its coupling to the leads. The resulting charged states should be a better representation of the states involved in tunneling transport in SET when Coulomb blockade is lifted.

We model the external potential by a simple Gaussian confining potential of the form

$$U = V_0 e^{-\alpha_x (x-x_0)^2 - \alpha_y (y-y_0)^2 - \alpha_z (z-z_0)^2}. \quad (5)$$

Here, V_0 is the magnitude of the potential centered at (x_0,y_0,z_0), which in our case is the position of the central Fe atom of the $\{Fe_4\}$. The constants α are the width of the potential along the corresponding directions and are chosen so that the potential drops quickly at distances larger than $\{Fe_4\}$. The sign of V_0 determines whether the extra electron will be confined into or repelled from the $\{Fe_4\}$ molecule. Thus, for the anion case a negative V_0 will attract the electron, whereas for the cation case a positive V_0 will attract the "hole" inside the molecule. The form of the potential given in Eq. (5) is admittedly not the most realistic representation of the potential generated by a gate electrode. It is chosen simply as a convenient expedient to mimic the effect of the gate in our finite-size system. In a real device, the main effect of a gate voltage is to control independently the chemical potential (that is, the energy levels) of the central island with respect to the chemical potentials of the bulk leads, which are essentially unaffected by the gate. In our finite system, where the leads themselves are nanoclusters, an extended planar charge distribution, which certainly is a more realistic representation of the gate electrode, would strongly affect also levels of the leads. Our choice of the gate potential realizes the wanted effect of the gate on the molecular levels.

We start by looking at the effect of the gate voltage on the anisotropy of the isolated $\{Fe_4\}$ SMM. We have first considered a gate voltage that depends only on the variable z. The resulting electric field points along the the z axis, which is the easy axis of the molecule.

From Fig. 11 we note that in the anion case a confining potential for the extra electron ($V_0 < 0$) reduces the anisotropy

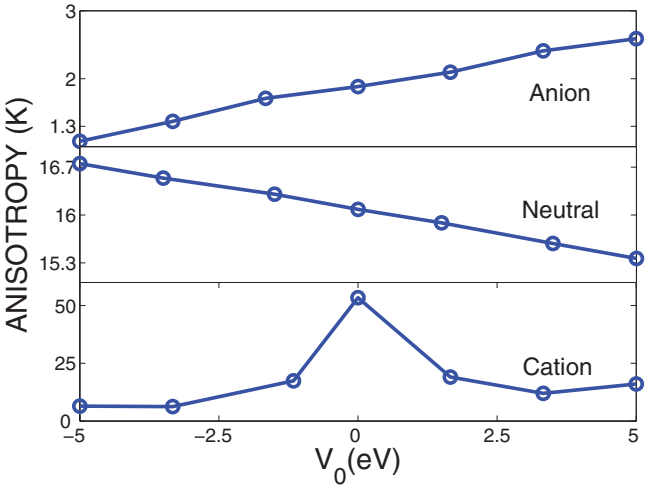

FIG. 11. (Color online) Variation of the magnetic anisotropy energy as a function of a confining potential V_0 applied along the C_3 axis (perpendicular to the plane of the $\{Fe_4\}$ triangle) of an isolated $\{Fe_4\}$ SMM.

TABLE IV. The effects of confining potential on neutral {Fe$_4$} SMM. Δ is the anisotropy energy and D and E are the parameters of the Hamiltonian (2), all in units of K. Here, the units of α are bohrs^2.

				Anisotropy		
V_0 (eV)	α_x	α_y	α_z	Δ (K)	D (K)	E (K)
0.0	0	0	0	16.06	−0.63	0.00
−5.0	0.01	0	0.01	17.00	−0.64	−0.03
−5.0	0.01	0	0	15.77	−0.60	−0.02

barrier, whereas repelling the extra charge away from the molecule increases the anisotropy. The neutral molecule displays an opposite behavior as a function of V_0. In both cases, the behavior of the anisotropy is close to a linear function of V_0. As expected, the variation of the anisotropy energy for the neutral molecule is limited, less than 10% for the largest applied voltage. The cation is special. We have seen that at zero voltage, the system has a large anisotropy barrier (see Table I) due to a quasidegeneracy at the Fermi level. The external potential lifts this degeneracy and the anisotropy energy decreases sharply for both signs of V_0.

The confining potential that we have applied above does not break the C_3 symmetry of the system and hence the parameter E in Eq. (2), characterizing the transverse component of the magnetic anisotropy, is zero. However, the symmetry can be broken by applying an electric field along directions other than the easy axis. Table IV shows the effect of this broken symmetry on the anisotropy of the isolated {Fe$_4$} SMM.

It is evident from Table IV that E is no longer zero if the electric field is applied along directions other than the easy axis. A nonzero E allows different eigenstates of the z component of the giant spin to mix with each other. A transverse component in principle can cause quantum tunneling of the molecule giant spin. Thus, this method can be used as electric control of magnetic properties. It can play a significant role in transport, for example, by modifying spin selection rules and by opening alternative channels via quantum tunneling of the magnetization.

We now discuss the effect of the applied gate voltage when the {Fe$_4$} molecule is attached to Au leads. In this case, we have applied the field only along the easy axis of the molecule attached to the leads of type 2, as shown in Fig. 4. We have seen in the previous section that since HOMO and LUMO states and states close in energy to these are primarily localized on the Au leads and phenyl linker, an added or removed electron leaves {Fe$_4$} largely unaffected. But, the presence of a confining potential ($V_0 < 0$ for electrons), applied only on the {Fe$_4$} part of the system, brings the states localized within {Fe$_4$} SMM closer to LUMO levels. Thus, when an electron is added to the system, the fraction of this extra charge that goes inside the molecule increases as we increase the confining potential. Similarly, when an electron is subtracted from the system, an applied positive gate voltage ($V_0 > 0$) tends to localize a fraction of the positive extra charge (a hole) closer to the molecule.

As an example, we consider the effect of a confining potential for the anion case ($Q = -1$, one electron added to the system). Figure 12 shows the change in fractional

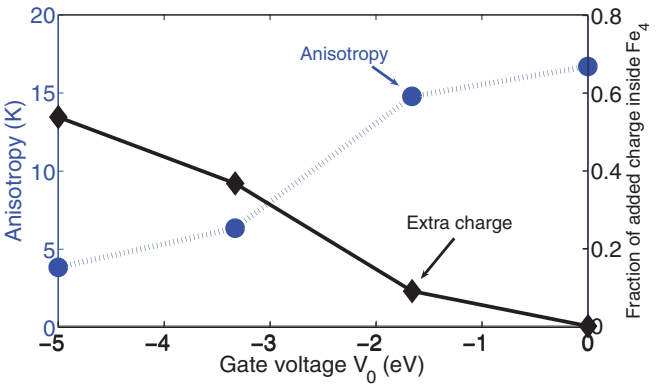

FIG. 12. (Color online) Fraction of the added charge (blue circles) confined inside {Fe$_4$}, as a function of the confining potential strength, and corresponding change in the magnetic anisotropy (black diamonds) of the leads plus molecule system in the anion state $Q = -1$. The external potential corresponds to an electric field along the z direction (see Fig. 4).

charge that enters into the {Fe$_4$} molecule as the strength of confining potential is increased, and the corresponding change in magnetic anisotropy energy of the system. Clearly, as the voltage is increased, more of the added electron is pushed inside the molecule. As the charge fraction approaches unity, the anisotropy decreases and converges to the value obtained for the anionic state of the isolated {Fe$_4$} SMM.

It turns out that not only the anisotropy energy, but other magnetic properties converge to the properties of the anion state of the isolated {Fe$_4$} as the extra charge, under the effect of the external potential, moves closer to the center of the molecule. The easy axis of the system, which in the zero potential points perpendicular to the plane of the Fe$_4$ triangle and towards the leads, eventually rotates into the plane of the Fe$_4$ triangle, exactly as in the case of the anion state of the isolated {Fe$_4$} SMM. Similarly, as the added charge moves inside the inner magnetic core of {Fe$_4$}, the total spin of the system is reduced from $S = \frac{11}{2}$ to the value of the anion state of the isolated molecule $S = \frac{9}{2}$.

Similar results are obtained for the cation. As we apply an increasingly positive voltage, a larger fraction of a (negative) electron charge is pushed outside {Fe$_4$} or, equivalently, a larger fraction of (positive) hole is attracted inside the {Fe$_4$}. As a result, the anisotropy energy increases and it reaches a value of 22.8 K for $V_0 = 5$ eV, with more than half of the extra (positive) charge now inside {Fe$_4$}. Similarly, the spin also switches from $S = \frac{11}{2}$ at $V_0 = 0$ to $S = \frac{9}{2}$ at $V_0 = 5$ eV. Again, this is consistent with both the spin and the anisotropy converging towards the corresponding values of the isolated cation state.

A summary of the dependence of the anisotropy energy as a function of the external potential for all three charge states is shown in Fig. 13. While the anisotropy of the neutral state displays a weak dependence on the field, the anisotropy of the two charged states is significantly affected. These calculations demonstrate that, for a SET with a {Fe$_4$} SMM as a central island, by manipulating the position of the additional charge with a gate voltage, it is possible to modify the magnetic

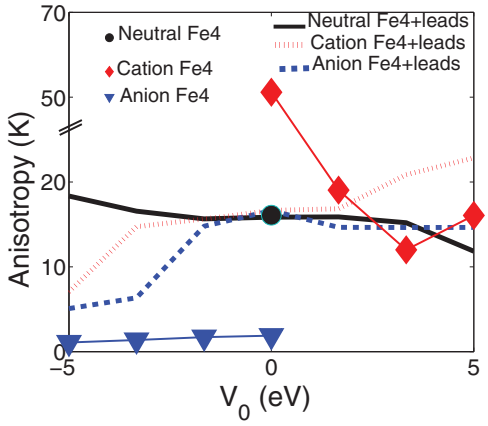

FIG. 13. (Color online) Magnetic anisotropy as a function of a confining field for the molecule plus leads (type-2) system, for the three charge states. The field is applied along the easy axis, that is, perpendicular to the plane of the molecule. The anisotropy for the the three charge states for the isolated molecule is included as a comparison (see diamond, circle, and triangle symbols).

properties of the SMM. This in turn can have important effects on the tunneling transport of the device.

VI. COMPARISON WITH SET EXPERIMENTS

Recent SET experiments[16,18] have permitted the first measurements of the magnetic characteristics of the $\{Fe_4\}$ SMM weakly coupled to Au leads, for both neutral and charged states. Comparison with our theoretical results has to be done with caution since important details (e.g., the type of linker used, see below) might differ in the two cases. In a first study, Zyazin *et al.*[16] have studied quantum transport in the inelastic cotunneling regime. By measuring the zero-field splitting of magnetic excitations and their dependence on the magnetic field, it was possible, with the help of the model Hamiltonian of Eq. (2), to extract values of the giant spin S and the magnetic anisotropy energy $\Delta = DS^2$ for three adjacent charge states N (neutral), $N+1$ (anion), and $N-1$ (cation). For the neutral state, the spin of the molecule was found to be equal to expected value $S_N = 5$ and the anisotropy energy to be consistent with the value in the bulk phase, $\Delta_N = 1.4$ meV $= 16.24$ K. These results are in good agreement with our theoretical estimate for the $Q = 0$ charge state (see Table III).

For the charged states, the situation is more complicated. For the reduced molecule (anion state, one electron added), the experimental measurements gave $S_{N+1} = \frac{11}{2}$ for the spin and $\Delta_{N+1} = 2.7$ meV $= 31.30$ K for the anisotropy. For the oxidized molecule (cation state, one electron removed), the measurements gave $S_{N-1} = \frac{9}{2}$ and $\Delta_{N-1} = 1.8$ meV $=$ 20.90 K, respectively. Comparing these findings with the results of our calculations (see Table III), we can see that, for a given choice of lead type (type 1 or type 2), the theoretical value of the spin is consistent with the experimental one for either cation or anion, but not for both. We can also conclude that the experiment typically finds larger values for the anisotropy barrier, for both reduced and oxidized states, than the values predicted by theory.

Several reasons can be responsible for these discrepancies. First, the functionalization of the molecule used in the experiment is slightly different from the one used in the calculations. In fact, in the experiments, two different types of ligands were used. In one case (labeled as sample A), the $\{Fe_4\}$ SMM was connected to the Au lead by the phenyl group. In the second case (labeled as sample B), the $\{Fe_4\}$ was connected via a thiol group C_9S. The coupling molecule lead turns out to be weaker in sample A than in sample B.[46] As shown above, in all our calculations we have used a different type of linker, which was a combination of a phenyl group and a thiol group.

Second, in experiment, different charge states are achieved by adding or removing electrons to the central region of SET via a gate voltage. In the theoretical calculations, the two relevant charged states are constructed by adding or removing an electron to a system consisting of the $\{Fe_4\}$ connected to finite leads. The extra charge is allowed to relax in the self-consistent field, and it occupies regions away from the $\{Fe_4\}$, which affects the magnetic properties of the system. Indeed, confining the extra charge on the SMM with an external gate modifies the anisotropy barrier.

Third, the evaluation of the magnetic properties from experiment done in Ref. 16 relies on the use of the model Hamiltonian of Eq. (2). The fitting of the experimental results maintains a degree of uncertainty and arbitrariness. For example, although in the experiment three different adjacent charge states are detected, it is not possible to establish uniquely the absolute charge state at a given gate. In other words, it not possible to be sure whether $V_g = 0$ corresponds to the neutral case. This implies an uncertainty in the choice of the corresponding spin Hamiltonian. Furthermore, the extraction of a spin Hamiltonian could be problematic in cases of level degeneracy at the Fermi level, not uncommon for charged states. In this case, we have seen the the giant-spin model of Eq. (2) might become inadequate.

Finally, the method of Ref. 16 relies on the measurement of inelastic cotunneling excitations, which is quite sensitive to the coupling between molecule and leads, and therefore it is a procedure not immune of uncertainties. Indeed, in a more recent paper, Burzurí *et al.*[18] introduced a novel gate-voltage spectroscopy technique which permits the measurement of the anisotropy of an individual SMM in different charge states by tracking the dependence of the charge degeneracy point as a function of magnetic field. This method is much more sensitive and accurate than the method based on conventional transport spectroscopy employed in Ref. 16. The spin Hamiltonian provides a good fit of the data if $S_N = 5$, $\Delta_N = 16.2$ K for the neutral state, $S_{N+1} = \frac{9}{2}$, and $\Delta_{N+1} = 16.0$ K for the reduced state and $S_{N-1} = \frac{11}{2}$ and $\Delta_{N-1} = 16.5$ K for the oxides state. Furthermore, the orientation of the easy axis is found to exhibit only small variations among different charge states. Although some details might differ,[47] these results are quite consistent with the small variations in anisotropy magnitude and the unchanged orientation of the easy axis that we find for the three charge states in our theoretical analysis (see Table III).

As we mentioned above, the small variation in the anisotropy for different charged states found in our calculations is related to the fact that any extra charge added to the molecule + leads system tends not to reside directly on the

magnetic atoms, but mainly on the ligands and on the Au leads. We pointed out that this could be, in part, an artificial effect due to the way we constructed charged states in our finite-size system and to the delocalizing character of our DFT approach. On the other hand, it is interesting that our estimates for the magnetic anisotropy are essentially consistent with the experimental results of Ref. 18, which are obtained exactly at charge degeneracy points. At these special values of the external gate voltage, the energy of two adjacent charge states is the same. We can imagine that at the degeneracy point the extra charge can swap energy-free from the electrodes and the molecule and might be localized primarily in a region where the molecule is connected to the leads. If this were the case, the charge distribution shown in Fig. 9 could be in fact a more realistic description of the charge states than previously anticipated. We could also surmise that, exactly as it happens in our calculations when we apply an external confining potential, changing the gate voltage to move away from the degeneracy point and make a given charge state more stable could strongly affect the the magnetic anisotropy. Indeed, the results of the the first experiment,[16] where the anisotropy was not extracted at degeneracy points but in the middle of a Coulomb blockade diamond, show a significantly enhanced anisotropy for charged states. The two experimental results could simply indicate that in one case the extra charge is localized closer to the SMM than in the other, exactly as it happens in our theoretical modeling.

VII. CONCLUSIONS

In this paper, we have studied the electronic and magnetic properties of a {Fe_4} SMM in a single-electron transistor (SET) geometry, using DFT as implemented in NRLMOL. We have modeled the system by a {Fe_4} functionalized with phenyl groups attached to two metal leads described by Au_{20} nanoclusters. Our calculations show that the magnetic structure of the neutral {Fe_4} SMM, that is, its spin ordering and magnetic anisotropy, remains stable in the presence of metallic leads. Specifically, the ground-state spin is $S = 5$ and the anisotropy energy is of the order of 16 K, as for the isolated {Fe_4}. This result is ascribed to the fact that, when attaching leads to {Fe_4}, any charge transfer between the molecule and the metal leads occurs primarily in the contact region and on the ligands, but does not involve the magnetic core of the molecule.

Based on the properties of the HOMO and LUMO of the neutral system, when an electron is added to or subtracted from the molecule-lead system, we find that the added charge ($Q = \mp 1$) is primarily located on the ligands and on the leads. As a result, while the total spin of this finite system changes by $\Delta S = \pm\frac{1}{2}$, the magnetic anisotropy displays small variations both in magnitude and orientation with respect to the neutral state. In contrast, the anisotropy of the anion and cation states of an isolated {Fe_4} is quite different from the values of the neutral molecule since the added extra charge penetrates the region of the Fe atoms. The theoretical study of charged states $Q = \pm 1$ for the molecule-lead system is technically challenging, due to occurrence of small HOMO-LUMO gaps and consequent fractional occupancies of the states around the Fermi level. Furthermore, DFT tends to overdelocalize any added charge in the peripheral parts of the system. Nevertheless, the analysis of these states presented here sheds light on the properties of a {Fe_4} SET when individual electrons are added or subtracted to the "quantum dot" by overcoming the Coulomb charging energy with a gate voltage.

We have shown that an external electric potential, modeling a gate voltage, can be used to manipulate the charge on the molecule-lead system and with that the magnetic properties of the device. In particular, for the two charged states $Q = \pm 1$ when the extra charge, under the effect of the potential, is progressively removed from the ligands-leads region into the magnetic core of the molecule, the magnetic properties converge to the properties of the anion and cation states of the isolated {Fe_4}. This is an example of the electric control of magnetism of a SMM in a SET. The charged states of the molecule-leads system in the presence of external fields studied in this paper can be used to construct the transition-matrix elements entering a quantum master equation describing tunneling transport in a SET. With the limitations inherent to the DFT approach mentioned above, these states incorporate charging effects for the SMM weakly coupled to metal leads.

We have compared the results of our numerical calculations with the results of two recent experimental studies of tunneling transport in a {Fe_4} three-terminal device in the Coulomb blockade regime.[16,18] This comparison must be made with caution since some important details (e.g., the precise atomic and electronic structure of the ligands) are different and might explain some of the discrepancies between theory and experiment that we find. Nevertheless, one of these experiments[18] finds that the anisotropy for the two charged states $Q = \pm 1$ displays only small variations in magnitude and orientation from the corresponding values of the neutral states, in agreement with our theoretical findings. Interestingly enough, the experimental values are extracted by tracking the dependence of the charge degeneracy point between two adjacent charged states as a function of the magnetic field. Our numerical calculations show that the essential independence of the magnetic anisotropy on the charged states is related to the position of the added charge being far away from the magnetic core of the molecule. Thus, the agreement between theory and experiment might indicate that for a {Fe_4} SET the charge of an added (subtracted) electron close to a charge-degeneracy point is primarily located on the ligands and in the contact region with the leads. If correct, this would be an example in which a magnetic property of SMM-based SET can provide information on the electronic properties of the charged states.

For molecule-lead systems with finite gaps, we expect our results to provide accurate predictions of experiment. However, for those cases where HOMO-LUMO gaps are very small and the electronic states at the Fermi level are partially occupied, further understanding will require variationally accounting for the electronic occupations along the lines suggested in Ref. 35.

Another point of view is that such fractionally occupied solutions are also strongly affected by self-interaction corrections and that accounting for such corrections will often significantly decrease the possibility of fractionally occupied solutions. Self-interaction corrections are also likely to provide a more complete understanding of the nature of charged states investigated in this paper. Addressing spin-dependent

conductance in macromolecular to mesoscale devices will require efficient solutions to these problems and renewed efforts at extracting quantitative model Hamiltonians for such systems.

The analysis of different charge states of a molecule attached to leads and their dependence on an external potential, carried out here, can be viewed as the first step to study transport in the Coulomb blockade regime combining *ab initio* and master-equation methods. Indeed, while it is not possible to read off current-voltage characteristics directly from the results presented here, the charge states constructed in this paper are the basic ingredients to calculate transition-matrix elements that enter in a master-equation formalism describing charge transport. This is the goal that we are presently pursuing, which will be the topic of a separate publication.

ACKNOWLEDGMENT

This work was supported by the Faculty of Natural Science and Technology at Linnaeus University, the Swedish Research Council under Grants No. 621-2007-5019 and No. 621-2010-3761, and the NordForsk research network 080134 "Nanospintronics: theory and simulations."

APPENDIX: SPIN-ORBIT INTERACTION: PERTURBATIVE METHOD

The starting points are the matrix elements of the spin-orbit interaction (SOI) operator

$$U(\mathbf{r},\mathbf{p},\mathbf{s}) = -\frac{1}{2c^2}\mathbf{s}\cdot\mathbf{p}\times\nabla\Phi(\mathbf{r}) \tag{A1}$$

($\mathbf{p}$ is the momentum operator; $\mathbf{s}$ is the electron spin operator; Φ is the Coulomb potential; and c is the speed of light), taken with respect to the unperturbed single-particle spinor wave functions $|\psi_{k\sigma}\rangle = |\phi_{k\sigma}\rangle|\chi_\sigma\rangle$, which are solutions of the SCF-approximation Schrödinger equation

$$H|\psi_{k\sigma}\rangle = \epsilon_{k\sigma}|\psi_{k\sigma}\rangle. \tag{A2}$$

Here, $\phi_{k\sigma}(\mathbf{r}) \equiv \langle\mathbf{r}||\phi_{k\sigma}\rangle$ is the orbital part of the wave function; the two-component spinors $|\chi_\sigma\rangle$, $\sigma = (1,2)$ are the eigenstates of $\mathbf{s}\cdot\hat{\mathbf{n}}$, where the unit vector $\hat{\mathbf{n}} = \hat{\mathbf{n}}(\theta,\varphi)$ is an arbitrary quantization axis.

The matrix elements can be written as[23]

$$\begin{aligned} U_{k\sigma,k'\sigma'} &= \langle\psi_{k\sigma}|U(\mathbf{r},\mathbf{p},\mathbf{s})|\psi_{k'\sigma'}\rangle \\ &= -i\sum_i \langle\phi_{k\sigma}|V_i|\phi_{k'\sigma'}\rangle\langle\chi_\sigma|s_i|\chi_{\sigma'}\rangle, \end{aligned} \tag{A3}$$

where the matrix elements of the operator $\mathbf{V} = (V_x, V_y, V_z)$ are defined as

$$\begin{aligned} &\langle\phi_{k\sigma}|V_x|\phi_{k'\sigma'}\rangle \\ &= \frac{1}{2c^2}\left(\left\langle\frac{\partial\phi_{k\sigma}}{\partial z}\middle|\Phi\middle|\frac{\partial\phi_{k'\sigma'}}{\partial y}\right\rangle - \left\langle\frac{\partial\phi_{k\sigma}}{\partial y}\middle|\Phi\middle|\frac{\partial\phi_{k'\sigma'}}{\partial z}\right\rangle\right), \end{aligned} \tag{A4}$$

with similar expressions involving cyclical permutations of x, y, and z. Note that Eq. (A4) avoids the time-consuming calculation of the gradient of the Coulomb potential, replacing it with the calculation of the gradient of the basis functions in which $\phi(\mathbf{r})$ is expanded. The above representation of the spin-orbit interaction arises by an integration by parts of the matrix element defined in Eq. (A4). It is similar to the form of spin-orbit interaction that comes out of the Dirac equation.

In the absence of an external magnetic field, the first-order perturbation-theory correction to the *total GS energy* caused by the SOI is zero because of time-reversal symmetry. The second-order correction is nonzero and can be written as

$$\Delta_2 = \sum_{\sigma\sigma'}\sum_{i,j} M_{ij}^{\sigma\sigma'} s_i^{\sigma\sigma'} s_j^{\sigma'\sigma}, \tag{A5}$$

where

$$s_i^{\sigma\sigma'} \equiv \langle\chi_\sigma|s_i|\chi_{\sigma'}\rangle \tag{A6}$$

and

$$M_{ij}^{\sigma\sigma'} \equiv -\sum_{k=\text{occ}}\sum_{k'=\text{unocc}} \frac{\langle\phi_{k\sigma}|V_i|\phi_{k'\sigma'}\rangle\langle\phi_{k'\sigma'}|V_j|\phi_{k\sigma}\rangle}{\epsilon_{k\sigma} - \epsilon_{k'\sigma'}}, \tag{A7}$$

where the sums over k and k' involve occupied and unoccupied states, respectively.

Equation (A5) is the central equation in the study of the magnetic anisotropy. Since the spin matrix elements $s_i^{\sigma\sigma'}$ depend on the orientation of the arbitrary axis of quantization $\hat{\mathbf{n}}$, so does also the total-energy shift. This is precisely the origin of the magnetic anisotropy brought about by SOI.

We now consider the case of a closed-shell molecule, a system with a well-defined highest occupied molecular orbital (HOMO) and lowest unoccupied molecular orbital (LUMO) gap in order to avoid problems with partial occupancy, with ΔN excess of majority spin electrons.

We have the important relation[23]

$$\langle\chi_1|s_i|\chi_1\rangle = -\langle\chi_2|s_i|\chi_2\rangle = \frac{\langle S_i\rangle}{\Delta N}, \tag{A8}$$

where $\langle S_i\rangle$ is the GS expectation value of the ith component of the total spin of the system for the given choice of the quantization axis. On the basis of our discussion of the giant-spin model, $\langle S_i\rangle$ can be reinterpreted as the expectation values of the components of the giant-spin operator $\mathbf{S}$ for the spin-coherent state $|S,\hat{\mathbf{n}}\rangle$ with $S = \Delta N/2$.

Using the resolution of the identity in spin space $\sum_\sigma |\chi_\sigma\rangle\langle\chi_\sigma| = 1$, we can write

$$\begin{aligned} \langle\chi_1|s_i|\chi_2\rangle\langle\chi_2|s_j|\chi_1\rangle &= \langle\chi_1|s_i s_j|\chi_1\rangle - \langle\chi_1|s_i|\chi_1\rangle\langle\chi_1|s_j|\chi_1\rangle \\ &= \langle\chi_1|s_i s_j|\chi_1\rangle - \frac{\langle S_i\rangle\langle S_j\rangle}{(\Delta N)^2} \end{aligned} \tag{A9}$$

and a similar expression for $\langle\chi_2|s_i|\chi_1\rangle\langle\chi_1|s_j|\chi_2\rangle$.

With the help of Eqs. (A8), (A9), and $\langle\chi_\sigma|(s_i)^2|\chi_\sigma\rangle = \frac{1}{4}$, Eq. (A5) takes the form

$$\Delta_2 = \alpha + \sum_{ij}\gamma_{ij}\langle S_i\rangle\langle S_j\rangle, \tag{A10}$$

where $\alpha = \sum_{ij}(M_{ii}^{12} + M_{ii}^{21})$ is a constant independent of the quantization axis. The anisotropy tensor γ_{ij} is given by

$$\gamma_{ij} = \frac{1}{(\Delta N)^2}\sum_{ij}\left(M_{ij}^{11} + M_{ij}^{22} - M_{ij}^{12} - M_{ij}^{21}\right). \tag{A11}$$

The tensor γ_{ij} can now be diagonalized by a unitary transformation and Δ_2 becomes

$$\Delta_2 = \alpha + A(\langle S'_x\rangle)^2 + B(\langle S'_y\rangle)^2 + C(\langle S'_z\rangle)^2 \quad \text{(A12)}$$

$$= \alpha + A\langle (S'_x)^2\rangle + B\langle (S'_y)^2\rangle + C\langle (S'_z)^2\rangle, \quad \text{(A13)}$$

where A,B,C are the eigenvalues of γ_{ij} and the S'_i are the three spin components rotated along its three principal axes [Eq. (A13) follows from Eq. (A12) thanks to the properties of spin-coherent states].

This expression for Δ_2 is exactly the expectation value $\langle S,\hat{\mathbf{n}}|\mathcal{H}|S,\hat{\mathbf{n}}\rangle$ of the quantum spin Hamiltonian

$$\mathcal{H} = \alpha + A(S'_x)^2 + B(S'_y)^2 + C(S'_z)^2 \quad \text{(A14)}$$

in the spin-coherent state $|S,\hat{\mathbf{n}}\rangle$. Equation (A14) is equivalent to Eq. (2) up to an irrelevant constant.

[1] A. R. Rocha, V. M. Garcia-Suarez, S. W. Bailey, C. J. Lambert, J. Ferrer, and S. Sanvito, Nat. Mater. **4**, 335 (2005).

[2] A. R. Rocha, V. M. Garcia-Suarez, S. Bailey, C. Lambert, J. Ferrer, and S. Sanvito, Phys. Rev. B **73**, 085414 (2006).

[3] M. Trif, F. Troiani, D. Stepanenko, and D. Loss, Phys. Rev. B **82**, 045429 (2010).

[4] W. Wernsdorfer and R. Sessoli, Science **284**, 133 (1999).

[5] L. Bogani and W. Wernsdorfer, Nat. Mater. **7**, 179 (2008).

[6] A. Candini, S. Klyatskaya, M. Ruben, W. Wernsdorfer, and M. Affronte, Nano Lett. **11**, 2634 (2011).

[7] D. Gatteschi, R. Sessoli, and J. Villain, *Molecular Nenomagnets* (Oxford University Press, Oxford, UK, 2006).

[8] H. B. Heersche, Z. de Groot, J. A. Folk, H. S. J. van der Zant, C. Romeike, M. R. Wegewijs, L. Zobbi, D. Barreca, E. Tondello, and A. Cornia, Phys. Rev. Lett. **96**, 206801 (2006).

[9] M.-H. Jo, J. E. Grose, K. Baheti, M. M. Deshmukh, J. J. Sokol, E. M. Rumberger, D. N. Hendrickson, J. R. Long, H. Park, and D. C. Ralph, Nano Lett. **6**, 2014 (2006).

[10] R. Sessoli, H. Tsai, A. Schake, S. Y. Wang, J. B. Vincent, K. Folting, D. Gatteschi, G. Christou, and D. N. Hendrickson, J. Am. Chem. Soc. **115**, 1804 (1993).

[11] M. Mannini, P. Sainctavit, R. Sessoli, C. Cartier dit Moulin, F. Pineider, M.-A. Arrio, A. Cornia, and D. Gatteschi, Chem.–Euro. J. **14**, 7530 (2008).

[12] S. Accorsi, A.-L. Barra, A. Caneschi, G. Chastanet, A. Cornia, A. C. Fabretti, D. Gatteschi, C. Mortalo, E. Olivieri, F. Parenti, P. Rosa, R. Sessoli, L. Sorace, W. Wernsdorfer, and L. J. Zobbi, J. Am. Chem. Soc. **128**, 4742 (2006).

[13] L. Gregoli, C. Danieli, A.-L. Barra, P. Neugebauer, G. Pellegrino, G. Poneti, R. Sessoli, and A. Cornia, Chem.– Eur. J. **15**, 6456 (2009).

[14] M. Mannini, F. Pineider, P. Sainctavit, C. Danieli, E. Otero, C. Sciancalepore, A. Talarico, M.-A. Arrio, A. Cornia, D. Gatteschi, and R. Sessoli, Nat. Mater. **8**, 194 (2009).

[15] M. Mannini, F. Pineider, C. Danieli, F. Totti, L. Sorace, P. Sainctavit, M. A. Arrio, E. Otero, L. Joly, J. C. Cezar, A. Cornia, and R. Sessoli, Nature (London) **468**, 417 (2010).

[16] A. S. Zyazin, J. W. G. van den Berg, E. A. Osorio, H. S. J. van der Zant, N. P. Konstantinidis, M. Leijnse, M. R. Wegewijs, F. May, W. Hofstetter, C. Danieli, and A. Cornia, Nano Lett. **10**, 3307 (2010).

[17] A. S. Zyazin, H. S. J. van der Zant, M. R. Wegewijs, and A. Cornia, Synth. Met. **161**, 591 (2011).

[18] E. Burzuri, A. S. Zyazin, A. Cornia, and H. S. J. van der Zant, Phys. Rev. Lett. **109**, 147203 (2012).

[19] Ł. Michalak, C. M. Canali, M. R. Pederson, M. Paulsson, and V. G. Benza, Phys. Rev. Lett. **104**, 017202 (2010).

[20] S. Barraza-Lopez, K. Park, V. García-Suárez, and J. Ferrer, Phys. Rev. Lett. **102**, 246801 (2009).

[21] C. D. Pemmaraju, I. Rungger, and S. Sanvito, Phys. Rev. B **80**, 104422 (2009).

[22] F. Rostamzadeh Renani and G. Kirczenow, Phys. Rev. B **85**, 245415 (2012).

[23] M. R. Pederson and S. N. Khanna, Phys. Rev. B **60**, 9566 (1999).

[24] J. Kortus, M. R. Pederson, T. Baruah, N. Bernstein, and C. Hellberg, Polyhedron **22**, 1871 (2003).

[25] A. V. Postnikov, J. Kortus, and M. R. Pederson, Phys. Status Solidi B **243**, 2533 (2006).

[26] M. R. Pederson and T. Baruah, *Handbook of Magnetism and Magnetic Materials*, edited by S. Parkin and H. Kronmullerr (Wiley, London, 2007), Chap. 9.

[27] M. R. Pederson and K. A. Jackson, Phys. Rev. B **41**, 7453 (1990).

[28] K. A. Jackson and M. R. Pederson, Phys. Rev. B **42**, 3276 (1990).

[29] T. Baruah and M. R. Pederson, Int. J. Quantum Chem. **93**, 324 (2003).

[30] K. Park and M. R. Pederson, Phys. Rev. B **70**, 054414 (2004).

[31] C. van Wllen, J. Chem. Phys. **130**, 194109 (2009).

[32] P. J. S. Schmitt and C. v Wullen, J. Chem. Phys. **134**, 194113 (2011).

[33] J. F. Janak, Phys. Rev. B **18**, 7165 (1978).

[34] A. Ruzsinszky, J. Perdew, G. I. Csonka, O. Vydrov, and G. Scuseria, J. Chem. Phys. **125**, 194112 (2006).

[35] M. R. Pederson and K. A. Jackson, Phys. Rev. B **43**, 7312 (1991).

[36] M. Weinert and J. W. Davenport, Phys. Rev. B **45**, 13709 (1992).

[37] M. Grumbach, D. Hohl, R. Martin, and R. Car, J. Phys.: Condens. Matter **6**, 1999 (1994).

[38] J. P. Perdew, K. Burke, and M. Ernzerhof, Phys. Rev. Lett. **77**, 3865 (1996).

[39] A. L. Barra, A. Caneschi, A. Cornia, F. Fabrizi de Biani, D. Gatteschi, C. Sangregorio, R. Sessoli, and L. Sorace, J. Am. Chem. Soc. **121**, 5302 (1999).

[40] J. Ribas-Arino, T. Baruah, and M. R. Pederson, J. Chem. Phys. **123**, 044303 (2005).

[41] The anisotropy "barrier" for this case, mentioned in Table I, defined as the difference between the energy along the hard Z axis and the energy in the XY plane, should more properly be called magnetic anisotropy energy.

[42] J. Li, X. Li, H.-J. Zhai, and L.-S. Wang, Science **299**, 864 (2003).

[43] H. Häkkinen, Chem. Soc. Rev. **37**, 1847 (2008).

[44] The fact that in Table III the spin magnetic moment of the $Q = -1$ charge state is not exactly equal to an integer is due to the fractional occupancy (approximately 15%) of the spin-down LUMO in our

calculations, carried out with a finite smearing of the Fermi-Dirac distribution.

[45]Note, however, that the amplitude of the LUMO wave function is quite small in the central region. Therefore, an electron tunneling in from one of the leads would still find a bottleneck when tunneling out to the other lead.

[46]Note that in Ref. 16, the results reported for the anion and cation were obtained for samples A and B, respectively.

[47]In general, in Ref. 18 it is found that upon reduction, either from $N \rightarrow N+1$ or from $N-1 \rightarrow N$, the spin S always *decreases* and the anisotropy parameter D, defined via $\Delta = DS^2$, always *increases*. The results of our calculations (see Table III) show that both the anion and the cation have preferably $S = \frac{11}{2}$ for a lead of type 2, whereas $S = \frac{9}{2}$ for a lead of type 1. However, states with swapped spin configurations $S = \frac{11}{2} \leftrightarrow S = \frac{9}{2}$ are quite close in energy for both charged states.